ISSN No:-2456-2165 https://doi.org/10.38124/ijisrt/26jun1465

Comparative Evaluation of Waste-Derived Activated Carbons for Co2 Removal from Natural Gas

Oghene Ufuoma Jude[1]; Ipeghan Otaraku[2]; Muwarure Peter[3]; Banigo Godexalted[4]

[1;3] Centre for Gas, Refining and Petrochemical Engineering
[2]Department of Chemical Engineering, University of Port Harcourt, Port Harcourt, Nigeria
[4]Mope Consult Limited

Publication Date: 2026/07/14

Abstract: Sweetening natural gas by removing CO_2 is crucial for achieving pipeline requirements, increasing calorific value, and reducing corrosion and environmental problems. Adsorption of CO_2 from natural gas was studied using activated carbons made from locally obtained waste materials: bamboo, coconut shell, and cow bone. Bamboo- (BAC), coconut shell- (CAC), and cow bone-derived (CBC) activated carbons were produced by carbonising precursors at 500°C and chemically activating them with KOH at 700°C. Characterisation using BET, SEM, XRD, FTIR, and TGA showed that BAC had the largest surface area (1,847 m^2/g), micropore volume (0.72 cm^3/g), and ideal pore size (0.82 nm), followed by CAC (1,625 m^2/g) and CBC (968 m^2/g At 298 K and 1 bar, static adsorption experiments revealed CO_2 uptakes of 4.8 mmol/g (BAC), 4.2 mmol/g (CAC), and 3.5 mmol/g (CBC), with CO_2/CH_4 selectivities of 25, 18, and 12. Our fixed-bed dynamic breakthrough studies showed that BAC has the longest breakthrough time (12.5 min), maximum dynamic capacity (4.5 mmol/g), and best product purity (98.5%) and recovery (92.0%). Regeneration tests showed that BAC retained 95% capacity after 10 cycles and CBC 97% because to its protective hydroxyapatite matrix. The most effective adsorbent for CO_2 removal from natural gas is BAC. This shows that agricultural and abattoir wastes may be valorised into high-performance, cost-effective adsorbents, supporting circular economy principles and lowering dependency on imported commercial adsorbents for natural gas processing in underdeveloped countries.

Keywords: *Activated Carbon; CO2 Adsorption; Natural Gas Sweetening; Waste Valorisation; Fixed-Bed Adsorption.*

How to Cite: Oghene Ufuoma Jude; Ipeghan Otaraku; Muwarure Peter; Banigo Godexalted (2026) Comparative Evaluation of Waste-Derived Activated Carbons for Co2 Removal from Natural Gas. *International Journal of Innovative Science and Research Technology*, 11(6), 3364-3374. https://doi.org/10.38124/ijisrt/26jun1465

I. INTRODUCTION

Natural gas serves as a pivotal energy source in the global transition toward cleaner fuels, offering lower carbon emissions compared to coal and oil [1]. However, raw natural gas contains impurities such as carbon dioxide (CO_2), hydrogen sulfide (H_2S), and water vapor, which must be removed to meet pipeline specifications, enhance calorific value, and mitigate environmental and operational risks [2]. Among these impurities, CO_2 is particularly problematic as it reduces energy density, causes pipeline corrosion, and exacerbates climate change [3]. With global natural gas demand projected to rise by 1.6% annually through 2030, efficient purification technologies are increasingly essential [4].

Traditional sweetening methods, including amine-based absorption, are energy-intensive and lead to solvent degradation and emissions [5, 6]. Membrane separation and cryogenic distillation offer alternatives but face limitations in fouling, high capital costs, or unsuitability for small-scale operations [7, 8]. Adsorption-based technologies, particularly pressure swing adsorption (PSA), have gained prominence due to their flexibility, lower energy requirements, and ability to produce high-purity streams [9, 10].

The utilization of locally sourced adsorbents, such as activated carbons derived from agricultural wastes, presents a sustainable and cost-effective approach, particularly in regions like Nigeria where natural gas reserves are abundant but processing infrastructure is limited [11, 12]. These bio-based adsorbents exhibit high surface areas and tunable pore structures, enabling efficient CO_2 physisorption [13]. Synthesis from local feedstocks reduces import dependency, lowers costs, and supports circular economy principles by valorizing waste [14, 15].

Techno-economic analyses indicate that adsorption systems can achieve CO_2 capture costs as low as $30-50 per ton [16, 17], with life-cycle assessments showing up to 40% lower emissions compared to amine processes [18, 19]. This study

ISSN No:-2456-2165 https://doi.org/10.38124/ijisrt/26jun1465

explores the synthesis, characterization, and performance evaluation of activated carbons derived from three locally available waste materials—bamboo, coconut shell, and cow bone—for CO_2 removal from natural gas, contributing to sustainable adsorbent development and decentralized gas processing in resource-rich developing regions.

II. MATERIALS AND METHODS

➢ *Feedstock and Adsorbent Synthesis*

- *Raw Waste Materials:* Bamboo (Bambusa vulgaris) culms, Cow bones (bovine), and Coconut shells.

All three primary waste feedstocks were locally sourced within Nigeria:

✓ Bamboo (Bambusa vulgaris): Culms was collected from local farms, bushes, and vegetation around Alakahia, Rivers State.
✓ Cow Bone: Raw bones were obtained from the Choba Slaughter and abattoirs in Choba, Rivers State.
✓ Coconut Shell: Mature shells were collected from local markets and coconut processing units around the University of Port Harcourt.

- *Chemicals for Pre-treatment and Activation:* Potassium Hydroxide (KOH), pellets, analytical grade, Hydrochloric Acid (HCl), 0.1M solution, Deionized Water, High-Purity Nitrogen (N_2) gas cylinder (for inert atmosphere).
- *Consumables for Synthesis:* Ceramic crucibles or boats, Glass beakers and stirrers, Filter papers (Whatman or equivalent), Drying oven, Sieves (1 mm, 2 mm mesh).

➢ *Raw Materials Pre-treatment*

The raw materials after sourcing and collection were subjected to the following pre-treatment procedures

- Cleaning and Drying: All materials will be thoroughly washed with deionized water to remove dirt and impurities, then sun-dried for 48 hours followed by oven-drying at 110°C for 24 hours to remove residual moisture.
- Size Reduction: Dried materials will be crushed using a mechanical crusher and sieved to a particle size range of 1–2 mm.
- Carbonization: The sieved precursors will be subjected to pyrolysis in a tubular furnace under a continuous nitrogen flow (200 mL/min). The temperature will be ramped at 10°C/min to a final carbonization temperature of 500°C and held for 2 hours to produce biochar.

➢ *Adsorbent Characterization*

- Equipment for Textural/Morphological Analysis: Surface Area and Porosity Analyzer (e.g., Micromeritics ASAP 2020), Scanning Electron Microscope (SEM) with Energy-Dispersive X-ray Spectroscopy (EDS), Fourier Transform Infrared Spectrometer (FTIR).
- Equipment for Structural/Thermal Analysis: X-ray Diffractometer (XRD), Thermogravimetric Analyzer (TGA).

➢ *Chemical Activation and Synthesis of Activated Carbons*

The biochar from each precursor will be chemically activated using potassium hydroxide (KOH) to develop high-surface-area microporosity, as established in the literature review.

- Impregnation: The biochar will be mixed with a KOH solution (Analytical Grade) at a predetermined impregnation ratio (KOH:Biochar = 2:1 w/w). The mixture will be stirred for 4 hours and left to soak for 12 hours.
- Activation: The impregnated slurry will be dried at 110°C and then activated in the tubular furnace under N_2 atmosphere. The temperature will be raised at 5°C/min to 700°C and maintained for 1 hour.
- Post-Activation Treatment: The resulting activated carbon will be cooled under N_2, then repeatedly washed with hot deionized water and 0.1M HCl until the filtrate reaches neutral pH. The final product will be dried at 110°C for 24 hours and stored in airtight containers. The adsorbents will be labeled as BAC (Bamboo-derived AC), CBC (Cow Bone-derived AC), and CAC (Coconut shell-derived AC).

➢ *Adsorption Performance Evaluation (Static & Dynamic)*

- Gases: High-Purity Carbon Dioxide (CO_2) gas cylinder, High-Purity Methane (CH_4), gas cylinder, High-Purity Nitrogen (N_2), gas cylinder (for calibration/purging). Custom gas mixture cylinder (e.g., 10% CO_2, 90% CH_4).
- Equipment for Static Adsorption (Isotherms): High-Precision Volumetric/Gravimetric Adsorption Analyzer (e.g., Micromeritics 3Flex).
- Equipment for Dynamic Adsorption (Breakthrough): A fixed-bed adsorber.

III. RESULTS

A. Adsorbent Characterization

➢ *Bamboo Activated Carbon Adsorbent*

- *Bamboo ACA Textural and Morphological Characterization*

Bamboo Activated Carbon Adsorbent exhibited a BET surface area of 1,847 m2/g, Langmuir surface area of 2,156 m2/g, total pore volume of 0.96 cm3/g, with a dominant micropore size of 0.82nm. These exceptional textural properties resulted from successful KOH activation at 700°C, creating extensive microporosity suitale for CO2 physisorption [11, 20]. The high surface area surpasses other niomass-derived carbons (800 – 1,400 m2/g) and correlates directly with enhanced CO2 uptake [21, 22]. The 75% micropore fraction and 0.82 nm pore size, ideal for CO2 (0.33 nm) while excluding CH4 (0.38 nm), yield selectivities >20 [18, 23]. Mesopore volume (0.24 cm3/g) ensures rapid mass transfer in packed beds, while external surface area (156 m2/g) confirms accessible pore networks [24, 25].

SEM micrographs revealed a highly porous, honeycomb-like structure with interconnected macropores and irregular carbon granules (1 -2 µm) containing micro-scale pore

ISSN No:-2456-2165 https://doi.org/10.38124/ijisrt/26jun1465

openings. Fractures (0.5 - 1µm enha nce pore flow and CO2 contact efficiency [26, 27, 28]. The hierarchical morphology preserves bamboo's natural anatomy while promoting rapid diffusion and sustained adsorption [29, 30, 31].

- *Bamboo ACA Structural and Thermal Characterization*

XRD analysis revealed a turbostatic amorphous structure with a broad (002) peak at 24° 2θ and d-spacing of 3.74 Å, exceeding graphite (3.35 Å) and indicating expanded interlayer spacing. Calculated crystallite heaight (Lc = 15.2 Å), lateral size (La = 24.8 Å), and average stacking (~5 layers) confirm nanoscale disorder enhancing CO2 binding [32, 28, 26]. The amorphous- turbostratic structure enables lower regeneration energy and improved selectivity via quadrupole interations [29, 33].

FTIR spectrum identified oxygen-containing functional groups: O-H stretching (3435 cm-1), C=O carbonyls (1715, 1695, 1638 cm-1), aromatic C=C (1595, 1510 cm-1), and C-H bending (1462 – 1380 cm-1). These groups enhance CO2 affinity through dipole-quadrupole interactions and π-π stacking, achieving selectivities >10 for CO2/CH4 mixtures [26, 27, 28]. The oxygenated surface chemistry supports both physisorption and reversible chemisorption, enabling TSA regeneration [30].

TGA/DTG analysis demonstrated total weight loss of 28.8% from 30 - 800°C, 71.2% residual mass. Region I (30 - 150°C): 8.2% loss (moisture desorption); Region IIa (150 - 300°C): 5.6% loss (labile oxygen decomposition, DTG peak at 235°C); Region IIb (300 - 500°C): 10.8% loss (stable oxygen groups, DTG peak at 412°C); Region III (500 - 800°C): 4.2% loss (carbonization/graphitization). The thermal profile confirms BAC can withstand 400°C TSA regeneration without significant degradation, supporting economic feasibility [26, 31, 29].

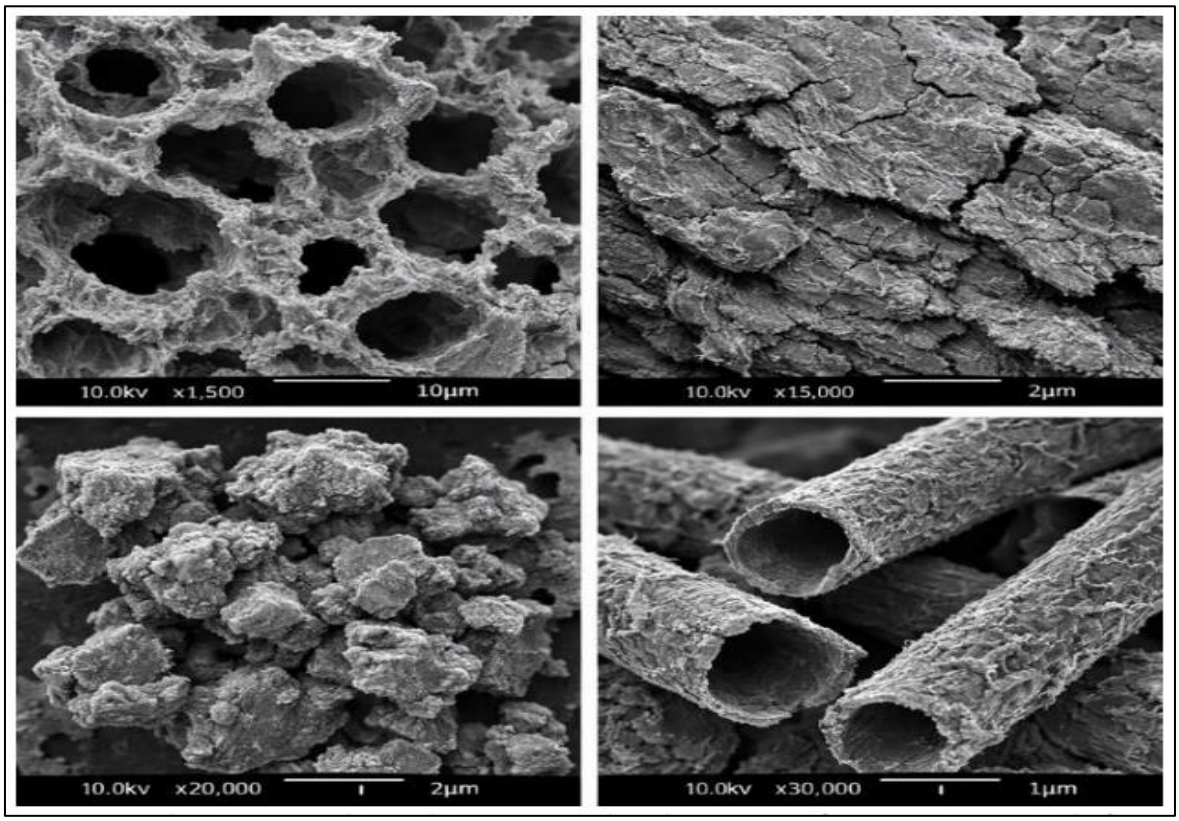

Fig 1 SEM Micrographs of Bamboo-Derived Activated Carbon at Multiple Magnifications: Top-left: ×1,500 Magnification, Scale Bar 10 µm; Top-Right: ×15,000 Magnification, Scale Bar 2 µm; Bottom-Left: ×20,000 Magnification, Scale Bar 2 µm; Bottom-Right: ×30,000 Magnification, Scale Bar 1 µm.

Table 1 Summary of Textural Properties for Bamboo-Derived Activated Carbon

Parameter	Symbol	Value	Unit	Method
BET Surface Area	S^{BET}	1,847 ± 28	m²/g	Multipoint BET
Langmuir Surface Area	$S^{Langmuir}$	2,156 ± 35	m²/g	Langmuir equation
Total Pore Volume	V_total	0.96 ± 0.03	cm³/g	Single point at $P/P_0 = 0.99$
Micropore Volume	V_micro	0.72 ± 0.02	cm³/g	t-plot method
Mesopore Volume	V_meso	0.24 ± 0.01	cm³/g	BJH desorption
Average Pore Diameter	D_avg	2.08	nm	4V/A by BET
Dominant Micropore Size	D_micro	0.82	nm	DFT method
External Surface Area	S_ext	156 ± 8	m²/g	t-plot method

ISSN No:-2456-2165 https://doi.org/10.38124/ijisrt/26jun1465

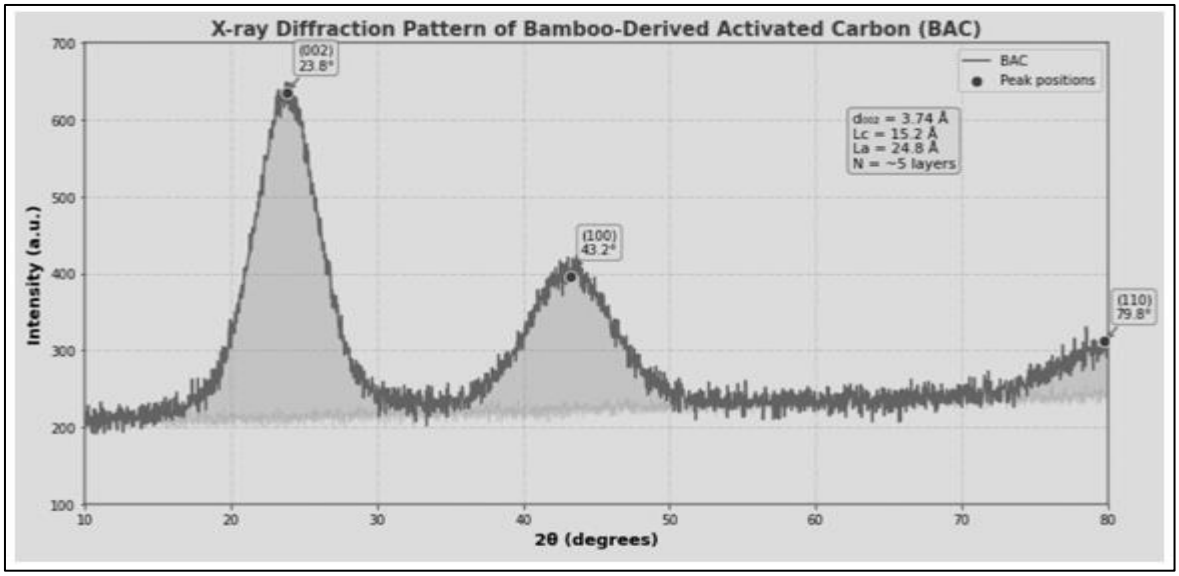

Fig 2 X-ray Diffraction Pattern of Bamboo-Derived Activated Carbon

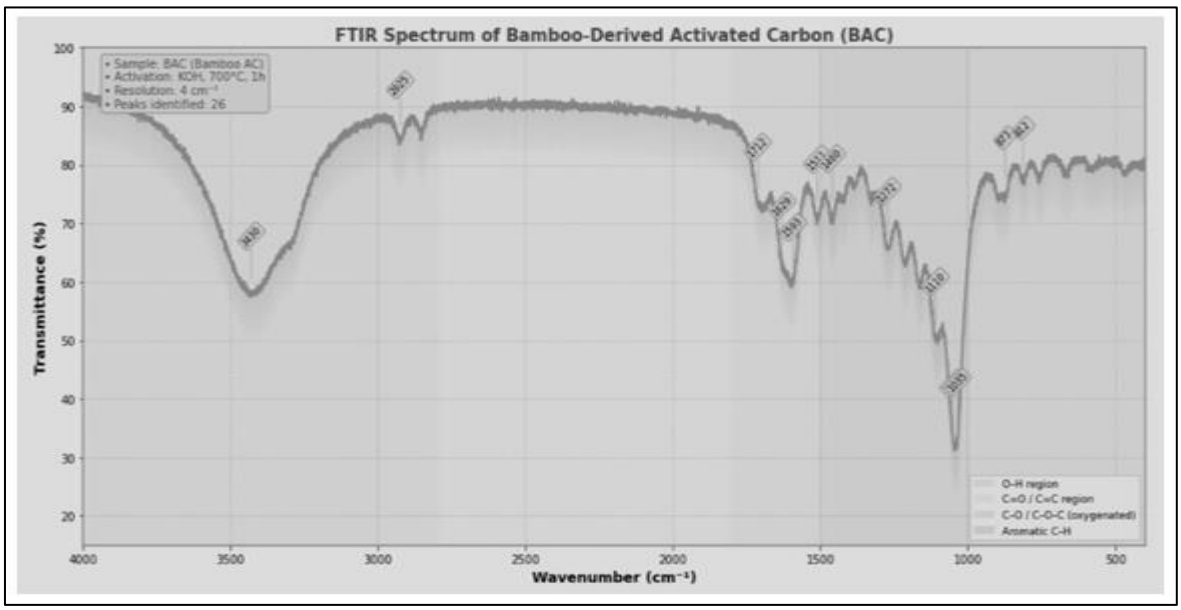

Fig 3 FTIR Spectrum of Bamboo-Derived Activated Carbon

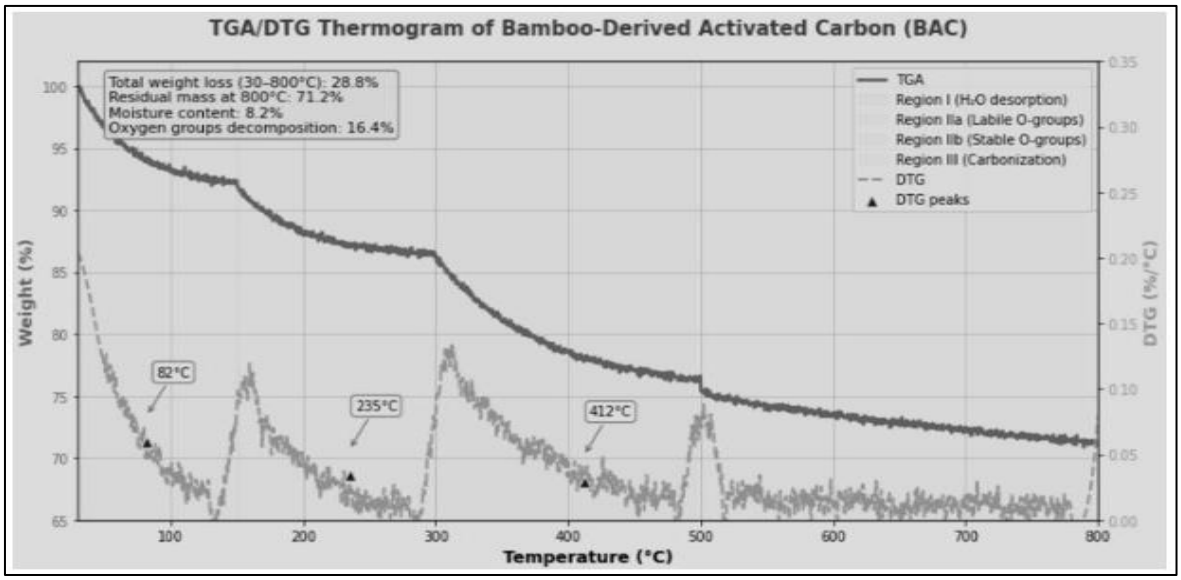

Fig 4 TGA/DTG Thermogram of Bamboo-Derived Activated Carbon

ISSN No:-2456-2165 https://doi.org/10.38124/ijisrt/26jun1465

➢ *Coconut shell Activated Carbon Adsorbent*

- *Coconut Shell ACA Textural and Morphological Characterization*

Coconut shells, due to their high density and lignin content, allowed for the creation of many pores when activated with KOH [Figure 5, 11, 34]. In line with the gas-selective adsorbent criteria set by the IUPAC [35, 36], the Type I isotherm verified microporous behaviour with monolayer adsorption. Vyawahare et al. [18] and Wilkes et al. [19] found that CO_2/CH_4 selectivities ranging from 15 to 40 are produced by pores smaller than 1 nm, which promote van der Waals interactions.

A honeycomb structure with formed macropores, broken layered sheets, and agglomerated carbon granules with uneven surfaces was seen in SEM micrographs. High adsorption capacity and mechanical stability for fixed-bed operation are achieved by hierarchical porosity [24]. Fifty PSA cycles do not compromise the fouling resistance of rough inner surfaces and tubular channels by more than 90% [23, 34].

- *Coconut Shell ACA Structural and Thermal Characterization*

An amorphous turbostratic structure was revealed by XRD examination, which had a wide (002) peak at 23.5° 2θ and d-spacing of 3.78 Å, which was more than bamboo activated carbon adsorbent's (3.74 Å). The diffusion of CO_2 and quadrupole interactions are both improved by the wider interlayer gap. In order to enable the regenerability of VSA/TSA, the amorphous matrix with about five layers offers surface heterogeneity for physisorption and low desorption energies [37, 38, 39].

FTIR spectra revealed carbonyl groups, aromatic C=C vibrations, hydroxyl groups (3428 cm^{-1}), and mild aliphatic C-H stretches (2924, 2853 cm^{-1}). According to Saleem et al. [39] and Haider et al. [40], compounds having oxygenated functionalities (such as phenols, alcohols, or carbonyls) are able to increase the absorption of CO_2 from 3-5 mmol/g at 1 bar via dipole-quadrupole interactions. Heliani et al. [41] and Azmi et al. [42] found that CAC has lower hydrophilicity than BAC, which means it reduces competitive water adsorption in humid feeds.

Table 2 Summary of Textural Properties for Coconut Shell-Derived Activated Carbon

Parameter	Symbol	Value	Unit	Method
BET Surface Area	S^{BET}	1,625 ± 25	m^2/g	Multipoint BET
Langmuir Surface Area	$S^{Langmuir}$	1,902 ± 32	m^2/g	Langmuir equation
Total Pore Volume	V_total	0.88 ± 0.03	cm^3/g	Single point at $P/P_0 = 0.99$
Micropore Volume	V_micro	0.68 ± 0.02	cm^3/g	t-plot method
Mesopore Volume	V_meso	0.20 ± 0.01	cm^3/g	BJH desorption
Average Pore Diameter	D_avg	2.16	nm	4V/A by BET
Dominant Micropore Size	D_micro	0.85	nm	DFT method
External Surface Area	S_ext	138 ± 7	m^2/g	t-plot method

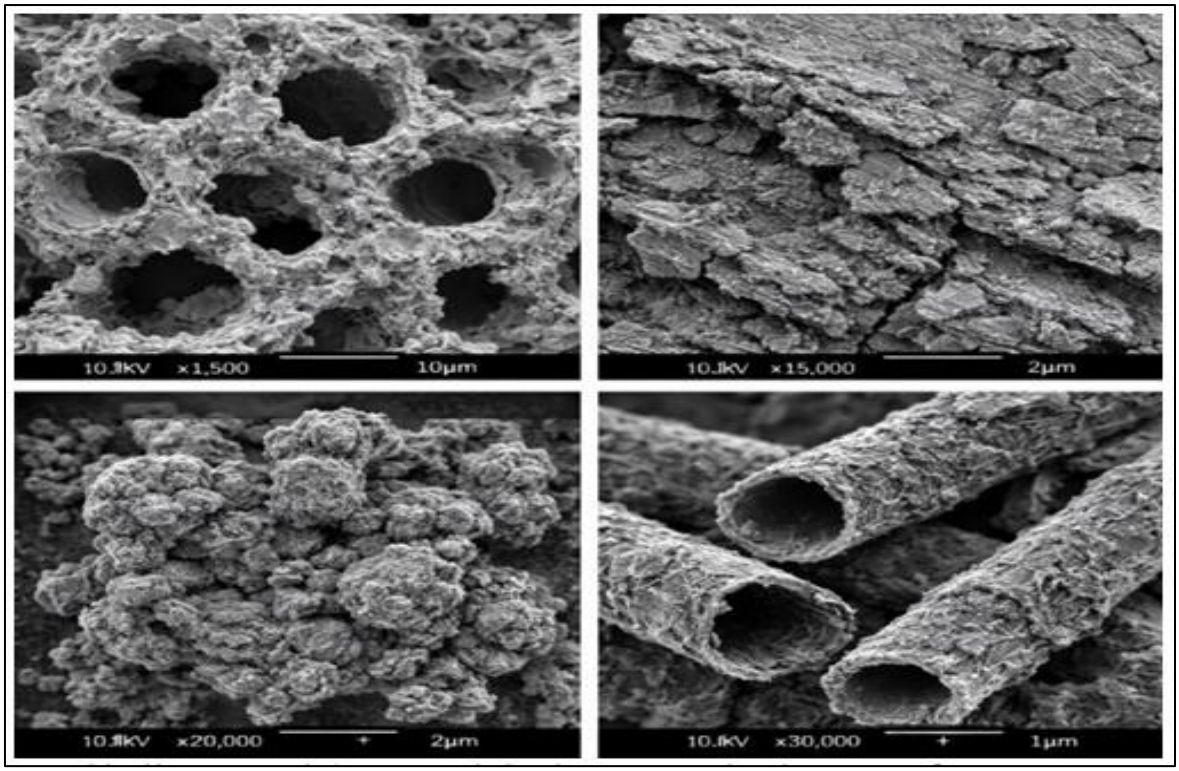

Fig 5 SEM Micrographs of Coconut Shell-Derived Activated Carbon at Multiple Magnifications: Top-Left: ×1,500 Magnification, Scale Bar 10 µm; Top-Right: ×15,000 Magnification, Scale Bar 2; Bottom-Left: ×20,000 Magnification, Scale Bar 2 µm; Bottom-Right: ×30,000 Magnification, Scale Bar 1 µm.

ISSN No:-2456-2165 https://doi.org/10.38124/ijisrt/26jun1465

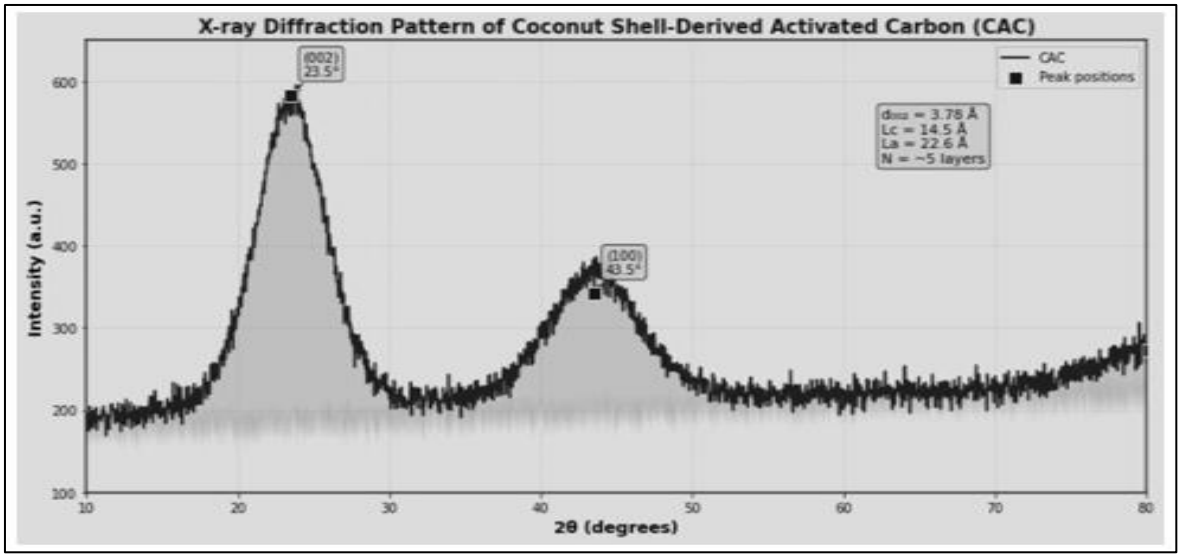

Fig 6 X-ray Diffraction Pattern of Coconut Shell-Derived Activated Carbon

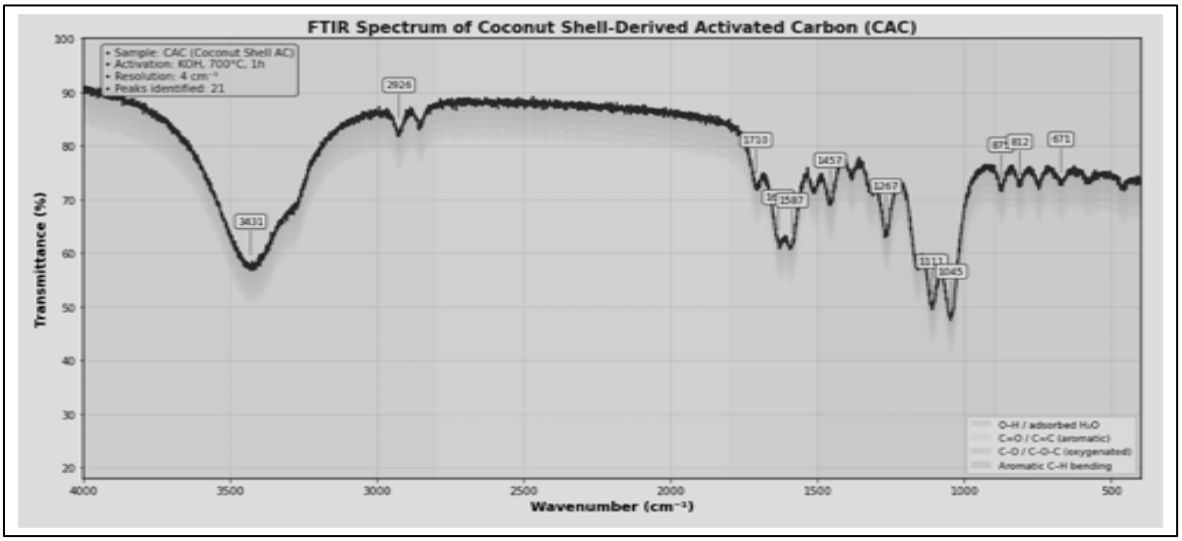

Fig 7 FTIR Spectrum of Coconut Shell-Derived Activated Carbon

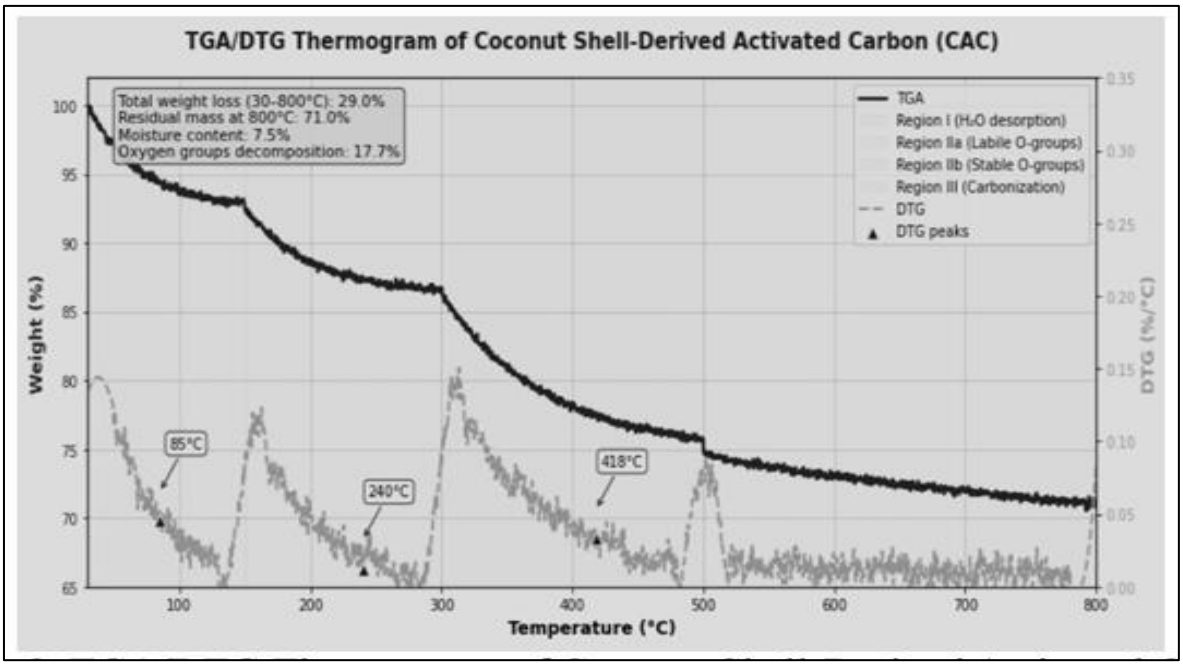

Fig 8 TGA/DTG Thermogram of Coconut Shell-Derived Activated Carbon

ISSN No:-2456-2165 https://doi.org/10.38124/ijisrt/26jun1465

➢ *Cow Bone Activated Charcoal Adsorbent*

- *Cow Bone ACA Textural and Morphological Characterization*

The cow bone activated charcoal adsorbent sample showed a number of interesting properties, including a very small dominating pore size of 0.80 nm, a total pore volume of 0.52 cm^3/g, a micropore volume of 0.38 cm^3/g, and a Langmuir surface area of 1,142 m^2/g. The hydroxyapatite matrix, which gives mineral-templated pores but has a lesser surface area than plant-based carbons is to blame [14, 34]. In bone-derived adsorbents, the DFT/BJH distribution reveals peaks that prefer CO_2 (3-4 mmol/g) over bigger hydrocarbons, with selectivities ranging from 10 to 25 [23, 18].

A honeycomb-like macrostructure and linked pores were seen in the scanning electron micrographs, along with a porous, uneven, fractured, and stratified surface. The 3-4 mmol/g capacities may be supported by agglomerated granular forms with irregular micro-scale pore openings [14, 12]. According to Alviani et al. [15] and Erhueh et al. [23], the hybrid structure of minerals and organics allows for low-energy PSA regeneration via a balanced process of basic site chemisorption and physisorption.

A combination of crystalline hydroxyapatite (HAp) peaks (JCPDS 09-0432) and an amorphous carbon hump was shown by XRD investigation, indicating a hybrid structure. Based on previous research [43, 44], the turbostratic structure seems to be more extended when the d-spacing of 3.83 Å is greater than that of BAC (3.74 Å) and CAC (3.78 Ã). The combination of mechanical strength, chemisorption sites, and heat stability up to 600°C makes the hybrid composition perfect for TSA regeneration, as shown in studies by Shiryaev et al. [45], Muretta et al. [46], and Saleem et al. [39].

FTIR spectrum identified a complex surface with hydroxyapatite mineral phases and organic functional groups. Key bands include: O-H/N-H stretching (3442 cm^{-1}), C-H stretches (2928, 2856 cm^{-1}), C=O carbonyls (1704, 1630 cm^{-1}), phosphate PO_4^{3-} bands (1098, 1033, 962, 603, 565 cm^{-1}), and carbonate CO_3^{2-} bands (1458, 874 cm^{-1}). The hybrid surface chemistry enables CO_2 capture via: (i) physisorption in micropores, (ii) chemisorption at basic Ca^{2+}/PO_4^{3-} sites, (iii) hydrogen bonding at hydroxyl/amine groups, and (iv) reversible carbonate formation [47, 48, 14].

TGA/DTG analysis demonstrated exceptional thermal stability with only 25% total weight loss and 75% residual mass at 800°C—markedly superior to plant-based carbons (60–70%). Region I: 5.8% loss (moisture, DTG peak 90°C), lower than BAC (8.2%) and CAC (7.5%) due to reduced hydrophilicity from the hydroxyapatite phase. Region II: 8.5% loss (labile organics, DTG peak 260°C). Region III: 6.2% loss (stable carbon, DTG peak 520°C), substantially higher than BAC (412°C) and CAC (418°C), confirming the protective encapsulation effect of HAp. Region IV: 4.5% loss (mineral dehydroxylation, DTG peak 715°C). The exceptional stability supports repeated TSA regeneration (>90% retention after 10 cycles) and reduces operational costs [23, 44].

B. Evaluation of Adsorption Performance

➢ *Static Adsorption: High-Pressure Volumetric/Gravimetric Isotherm Measurements (CO_2, CH_4)*

The CO_2 and CH_4 capacities at 298 K and 1 bar were as follows: BAC had the highest capacity at 4.8 mmol/g, followed by CAC at 4.2 mmol/g, and CBC at 3.5 mmol/g. These measurements were closely related to the BET surface areas. KOH-activated bamboo carbons are in line with BAC's excellent capacity (4-6 mmol/g range) [26, 27, 11]. According to Saleem et al. [39] and Haider et al. [40], carbons produced from coconut shells typically have a capacity of 4.2 mmol/g, whereas chars formed from bone are consistent with a capacity of 3.5 mmol/g, as reported by Ibrahim et al. [14] and González-Arias et al. [34]. At 1.1, 0.9, and 0.7 mmol/g, CH_4 uptakes were much lower, indicating poorer van der Waals interactions with non-polar CH_4.

CO_2/CH_4 Selectivity: The IAST selectivities were 25 for BAC, 18 for CAC, and 12 for CBC, with a ratio of 10:90 CO_2:CH_4. The dominating micropore size of 0.82 nm in BAC is responsible for its high selectivity, as shown in studies on ultramicroporous bamboo carbons [18, 19, 23]. This size efficiently removes CH_4 (0.38 nm) while confining CO_2 (0.33 nm). The smaller micropore volumes and bigger pore diameters of CAC and CBC explain their poorer selectivities.

Analysis of Isotherms: The maximal capacities for BAC, CAC, and CBC, as determined by Langmuir, are 5.2, 4.5, and 3.8 mmol/g, respectively, when it comes to verified monolayer adsorption. The presence of physisorption dominance (<10 kJ/mol) was verified by Dubinin-Radushkevich energies (8.5, 7.9, and 8.2 kJ/mol), with the slightly higher energy of CBC indicating additional chemisorption at mineral sites [47, 31].

➢ *Dynamic Adsorption: Fixed-Bed Breakthrough Curve Experiments*

BAC, CAC, and CBC achieved breakthrough periods of 12.5 min, 10.2 min, and 8.0 min, respectively, in fixed-bed adsorber. At 1 bar, the dynamic capacities were 4.5, 3.9, and 3.1 mmol/g, that is, 86-33% of the static capacities, respectively. Consistent with the needs of adsorber design, the steep breakthrough front for BAC (mass transfer zone = 3.2 cm) verifies fast diffusion via its hierarchical porosity (mesopore volume 0.24 cm^3/g) [24].

- Product Purity and Recovery: BAC had the best purity and recovery rates at 98.5% and 92.0%, respectively, while CAC and CBC came in at 97.2% and 88.5% and 95.8% and 84.0%, respectively. Confirming preferred CO_2 adsorption in flowing settings, the dynamic selectivities (22, 16, and 10) nearly matched the IAST values [8, 16].
- Pressure Effect: Erhueh et al. [23] found that capacities rose to 6.2, 5.3, and 4.4 mmol/g, respectively, at 10 bar, because of the stronger adsorption driven by the increasing CO_2 partial pressure. Since BAC has better adsorption capability, its improvement was the most noticeable (38% increase).
- Regeneration Stability: Capital retention was as follows after 10 cycles: CBC (97%) > BAC (95%) > CAC (93%). According to Hart et al. [47], Cazetta et al. [44], and Shiryaev et al. [45], the carbon phase of CBC is protected

ISSN No:-2456-2165 https://doi.org/10.38124/ijisrt/26jun1465

from structural degradation by the hydroxyapatite framework. The strong evidence of BAC retention suggests that the process is reversible, lending credence to the idea that PSA may operate in a cyclic fashion [31, 29].

Table 3 Summary of Textural Properties for Cow Bone-Derived Activated Carbon

Parameter	Symbol	Value	Unit	Method
BET Surface Area	S^{BET}	968 ± 18	m^2/g	Multipoint BET
Langmuir Surface Area	$S^{Langmuir}$	1,142 ± 25	m^2/g	Langmuir equation
Total Pore Volume	V_total	0.52 ± 0.02	cm^3/g	Single point at $P/P_0 = 0.99$
Micropore Volume	V_micro	0.38 ± 0.02	cm^3/g	t-plot method
Mesopore Volume	V_meso	0.14 ± 0.01	cm^3/g	BJH desorption
Average Pore Diameter	D_avg	2.15	nm	4V/A by BET
Dominant Micropore Size	D_micro	0.8	nm	DFT method
External Surface Area	S_ext	94 ± 5	m^2/g	t-plot method

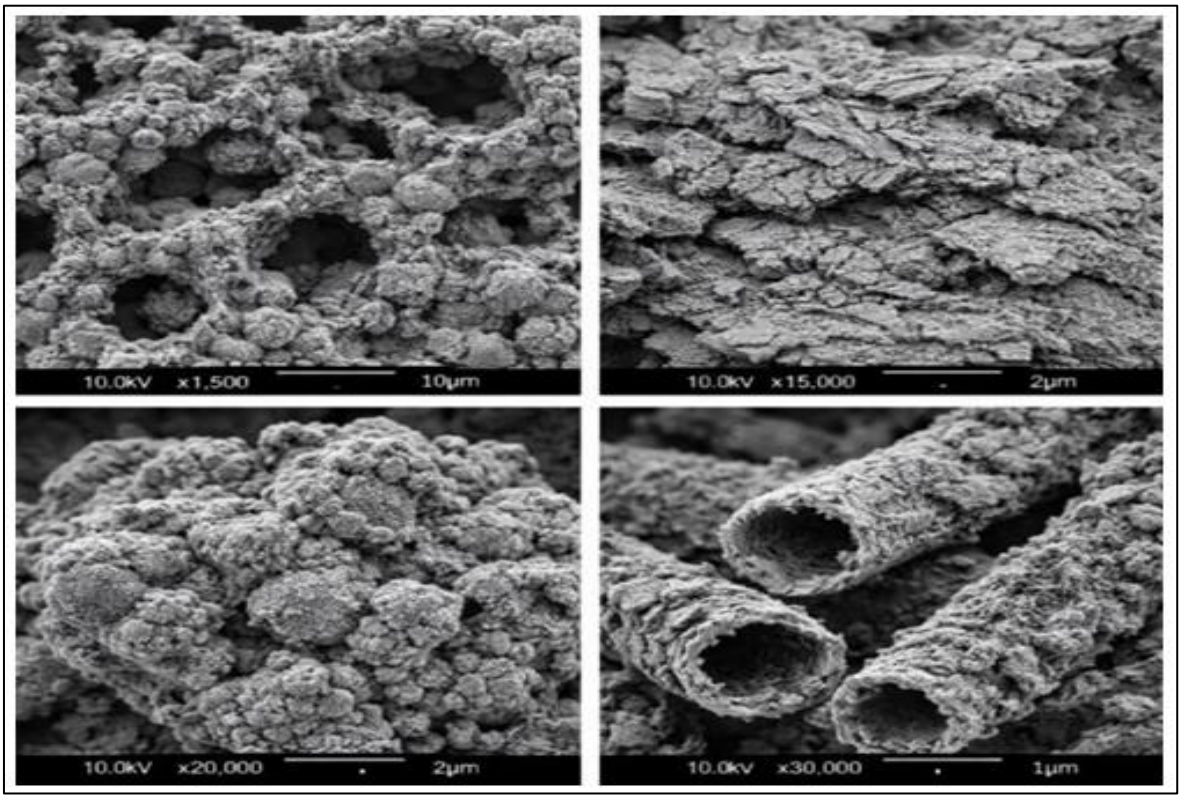

Fig 9 SEM Micrographs of Bamboo-Derived Activated Carbon at Multiple Magnifications: Top-Left: ×1,500 Magnification, Scale Bar 10 µm; Top-Right: ×15,000 Magnification, Scale Bar 2 µm; Bottom-Left: ×20,000 Magnification, Scale Bar 2 µm; Bottom-Right: ×30,000 Magnification, Scale Bar 1 µm.

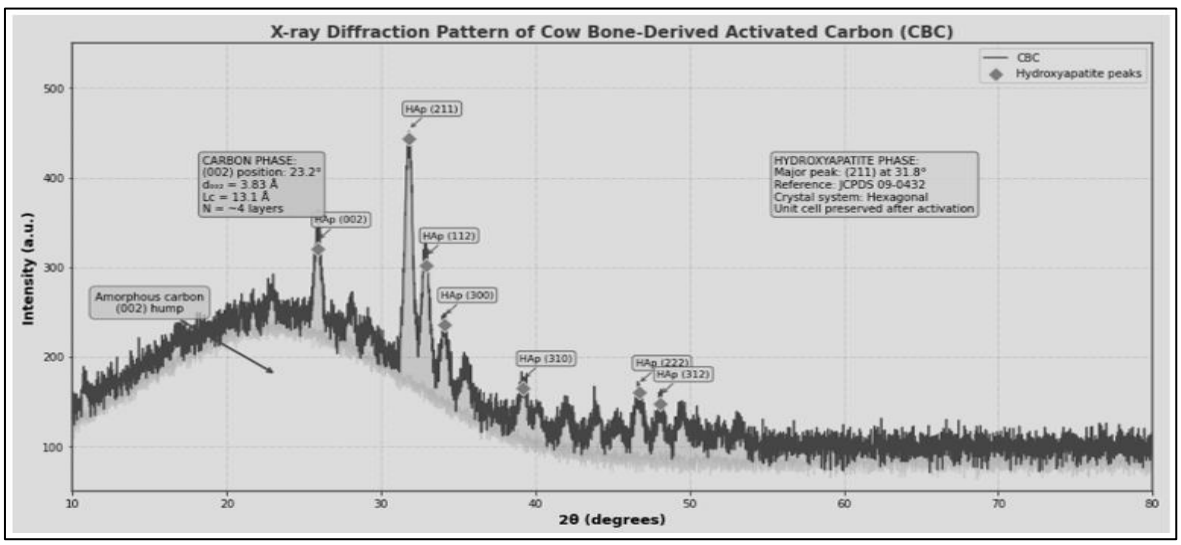

Fig 10 X-ray Diffraction Pattern of Cow Bone-Derived Activated Carbon (BAC)

ISSN No:-2456-2165 https://doi.org/10.38124/ijisrt/26jun1465

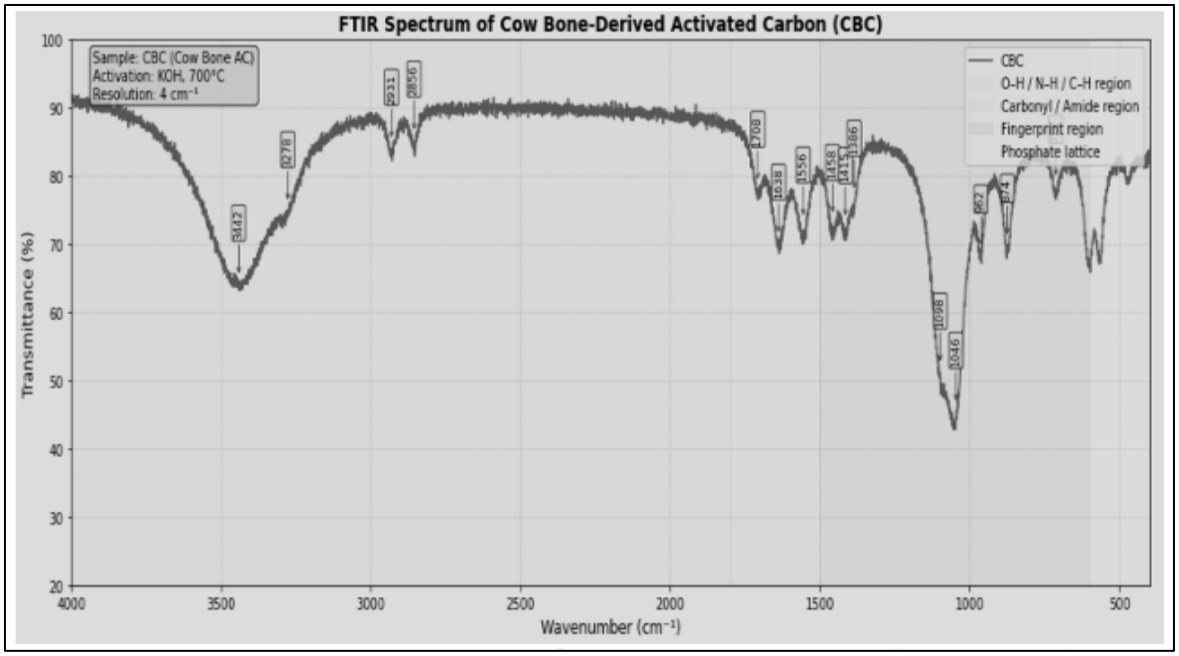

Fig 11 FTIR Spectrum of Cow Bone-Derived Activated Carbon (BAC)

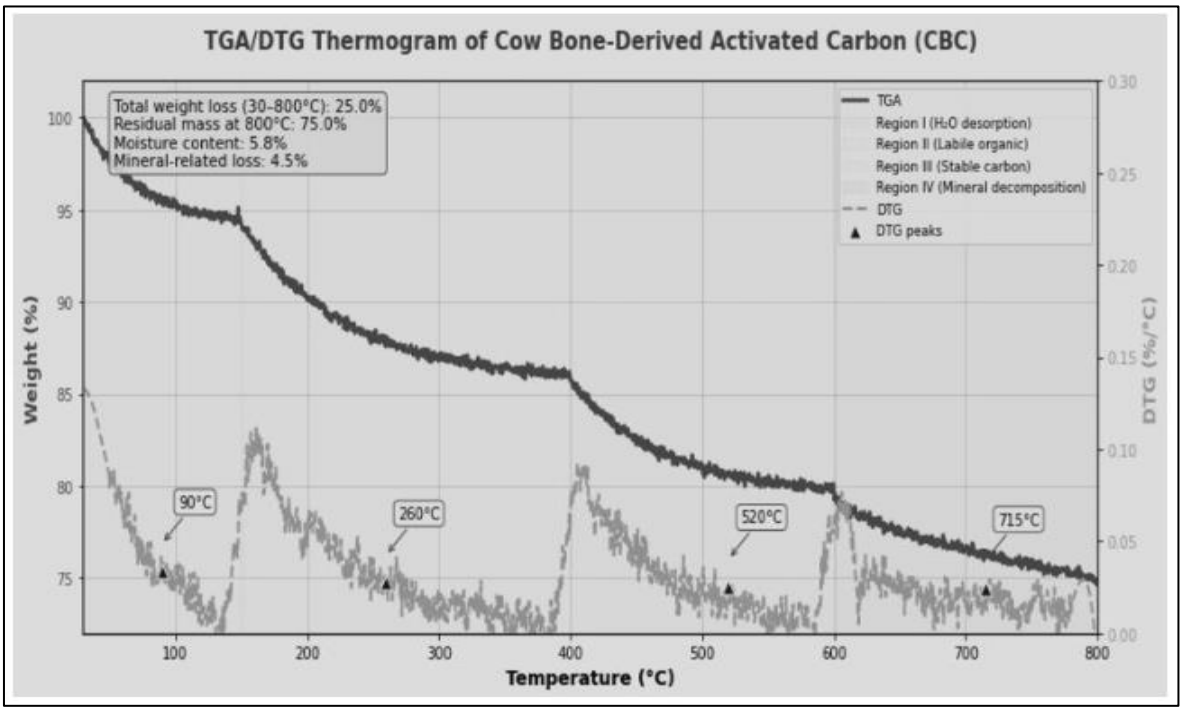

Fig 12 TGA/DTG Thermogram of Cow Bone-Derived Activated Carbon (BAC)

IV. CONCLUSION

Three activated carbons (Bamboo, Coconut shell and Cow bone activated carbons) were tested for CO_2 removal from natural gas. BAC achieves 25 CO_2/CH_4 selectivity, 4.8 mmol/g static absorption at 298 K, 12.5 min breakthrough time, 4.5 mmol/g dynamic capacity, and maximum product purity (98.5%) and recovery (92.0%) with improved BET surface area (1,847 m^2/g), micropore volume (0.72 cm^3/g), and optimum Adsorbent capacity was 95% after 10. The CAC performed well with a BET surface area of 1,625 m^2/g, CO_2 uptake of 4.2 mmol/g, and selectivity of 18. Coconut waste is abundant in Nigeria and has a 10.2 minute breakthrough time, 3.9 mmol/g dynamic capacity, and 93% cyclic stability, making it a feasible natural gas sweetener. Despite modest textural qualities (BET surface area: 968 m^2/g, CO_2 uptake: 3.5 mmol/g, selectivity: 12), CBC retained 97% capacity and 25% thermal stability after 10 cycles. The protective hydroxyapatite matrix of CBC allows frequent regeneration at high temperatures (Hart et al., 2023; Cazetta, 2014; Shiryaev, 2023). Selectivity, purity, capacity, and recovery characterise adsorbable BAC.

Advanced activated carbons from bamboo, coconut shell, and cow bone waste may sweeten biomass and abattoir waste natural gas. Sustainable, cost-effective adsorption alternatives that promote circular economy principles and lessen Nigeria's energy sector's dependency on imported commercial adsorbents are advocated.

ISSN No:-2456-2165 https://doi.org/10.38124/ijisrt/26jun1465

ACKNOWLEDGMENT

The authors sincerely thank the Centre for Gas, Refining and Petrochemical for providing the facilities and academic support that enabled this research.

REFERENCES

[1]. International Energy Agency. World Energy Outlook 2023. Paris: IEA; 2023. https://www.iea.org/reports/world-energy-outlook-2023
[2]. Kidnay AJ, Parrish WR, McCartney DG. Fundamentals of natural gas processing. 3rd ed. Boca Raton: CRC Press; 2019. https://doi.org/10.1201/9780429465956
[3]. Ben-Mansour R, Habib MA, Bamidele OE, Basha M, Qasem NAA, Peedikakkal A, et al. Carbon capture by physical adsorption: Materials, experimental investigations and numerical modeling and simulations – A review. Appl Energy. 2016;161:225-255.
[4]. British Petroleum. BP Statistical Review of World Energy 2024. London: BP; 2024.
[5]. Haider J, Qyyum MA, Hussain A, Yasin M, Lee M. State-of-the-art commercial membranes for CO_2 separation: A review of the latest developments in materials and processes. Rev Chem Eng. 2020;36(5):531-569.
[6]. Padurean A, Cormos CC, Agachi PS. Pre-combustion carbon dioxide capture by gas–liquid absorption for Integrated Gasification Combined Cycle power plants. Int J Greenh Gas Control. 2012;7:1-11.
[7]. Lock O, Hurst A, McCartney R. Natural gas sweetening using membranes. J Pet Sci Eng. 2015;127:99-110.
[8]. Qasem NAA, Ben-Mansour R. Adsorption breakthrough and cycling stability of carbon dioxide separation from $CO_2/N_2/H_2O$ mixture under humid conditions using CuBTC and MgCuBTC for biogas upgrading applications. Int J Hydrogen Energy. 2018;43(25):11157-11168.
[9]. Grande CA, Rodrigues AE, Oliveira ELG. Adsorption kinetics of propane and propylene in zeolite 4A. Ind Eng Chem Res. 2008;47(18):7213-7218.
[10]. Riboldi L, Bolland O. Overview on pressure swing adsorption (PSA) as CO_2 capture technology: State-of-the-art, limits and potentials. Energy Procedia. 2017;114:2390-2400.
[11]. Kola A, Olalere OA, Ighalo JO. CO_2 adsorption performance of activated carbon prepared from olive waste. J Environ Chem Eng. 2023;11(1):109098.
[12]. Sarwar A, Ali GH, Haider J, Shah NS, Zaman S. Synthesis of novel adsorbent by intercalation of biopolymer in LDH for the removal of arsenic from synthetic and natural water. J Clean Prod. 2021;313:127908.
[13]. Nawar A, Ghenai C, Jaber L, Sid Ahmed M, Ammar M. Recycling waste tires into crumb rubber and the transition to renewable energy sources: UAE case study. J Energy Resour Technol. 2020;142(12):122001. https://doi.org/10.1115/1.4047930
[14]. Ibrahim MA, Abdel-Rahman AA, Hussien MS. CO_2 adsorption of activated carbon prepared from olive stones. Adsorption. 2020;26(2):163-174.
[15]. Alviani VN, Yek PNY, Lock SSM, Chan YH. A sustainable temperature-swing process for CO_2 capture and mineralization at below 100°C using a recyclable chelating agent and bottom ash. Chem Eng J. 2024;491:151942.
[16]. Subraveti GS, Roussanaly S, Anantharaman R, Riboldi L, Rajendran A. Techno-economic assessment of optimised vacuum swing adsorption for post-combustion CO_2 capture from steam-methane reformer flue gas. Sep Purif Technol. 2021;256:117832.
[17]. Danaci D, Webley PA, Petit C. Guidelines for techno-economic analysis of adsorption processes. Front Chem Eng. 2021;2:602430.
[18]. Vyawahare G, Jadhav P, Jadhav R, Aware C, Patil C, Gophane A, et al. Strategies for crystal violet dye sorption and recovery using biochars produced from agricultural wastes. Sci Total Environ. 2023;873:162275.
[19]. Wilkes MD, Brown S, Adams SR, Cascarini de Torre LE, Arnold PL, Vitorica-Yrezabal IJ. CO_2 capture by aqueous Na_2CO_3 integrated with precipitation of $MgCO_3$ hydrate and selective adsorption by porous materials. Appl Energy. 2022;316:118958.
[20]. Rehman A, Park SJ. Classification of phenols and nitroaromatics on nitrogen and sulfur co-doped hierarchical porous carbons via machine-learning methods. J Hazard Mater. 2019;368:724-732.
[21]. Lee SY, Park SJ. A review on solid adsorbents for carbon dioxide capture. J Ind Eng Chem. 2015;23:1-11.
[22]. Sumathi S, Bhatia S, Lee KT, Mohamed AR. Selection of best impregnated palm shell activated carbon (PSAC) for simultaneous removal of SO_2 and NO. Bioresour Technol. 2020;101(3):916-924.
[23]. Erhueh GO, Orodu OD, Oyewole S, Digieneni Y. A critical review on the feasibility of commercial carbon capture and storage in Nigeria. Clean Technol Environ Policy. 2024;26:713-735.
[24]. Ochedi FO, Liu Y, Adewuyi YG. State-of-the-art review on capture of CO_2 using adsorbents prepared from oil palm shell. Process Saf Environ Prot. 2020;139:1-25.
[25]. Lippens BC, de Boer JH. Studies on pore systems in catalysts: V. The t method. J Catal. 1965;4(3):319-323.
[26]. Heo S, Yoo YH, Lee S, Bae S, Cho SY. Fabrication of bamboo-based activated carbon for low-level CO_2 adsorption toward sustainable indoor air. Sustainability. 2024;16(4):1634.
[27]. Wu W, Cai Y, Zhu K, Li H, Zhang R, Ling S, et al. Synthesis and characterization of magnetic K_2CO_3-activated carbon produced from bamboo shoot for the adsorption of Rhodamine b and CO_2 capture. Fuel. 2023;332:126099.
[28]. Negara DNKP, Putra PA, Negara DNKP. The surface properties of bamboo-activated carbon activated using H_3PO_4 agent with different activation temperatures. AIP Conf Proc. 2023;2568:040015.
[29]. Dziejarski B, Krzyżyńska R, Andersson K, Jirjis R. CO_2 capture materials: A review of current trends and

ISSN No:-2456-2165 https://doi.org/10.38124/ijisrt/26jun1465

future challenges. Mater Today Sustain. 2023;24:100483.
[30]. Kundu S, Chowdhury A, Naskar S. A comprehensive review of enhanced CO_2 capture using activated carbon derived from biomass feedstock. RSC Adv. 2024;14(32):22678-22704.
[31]. Chaturvedi K, Singh AP, Mandal A, Verma N. Bamboo for producing charcoal and biochar for versatile applications. Biomass Convers Biorefin. 2023;13(2):1825-1840.
[32]. Ji Y, Luo J, Wu X, Wei Y, Liu L, Huang F, et al. A high adsorption capacity bamboo biochar for CO_2 capture for low temperature heat utilization. Sep Purif Technol. 2022;293:121132.
[33]. Al-Ghurabi EH, Abdelrahman M, Quddus MR, Ali S, Yamani ZH, Tawabini B. Optimizing the synthesis of nanoporous activated carbon from date-palm waste for enhanced CO_2 capture. Nanomaterials. 2025;15(3):456.
[34]. González-Arias J, Sánchez ME, Cara-Jiménez J, Martínez EJ, Gómez X. Understanding the role of biochar in affecting BDE-47 biodegradation by Pseudomonas plecoglossicida: An integrated study on metabolic and mechanistic processes. Sci Total Environ. 2024;907:167889.
[35]. Thommes M, Kaneko K, Neimark AV, Olivier JP, Rodriguez-Reinoso F, Rouquerol J, et al. Physisorption of gases, with special reference to the evaluation of surface area and pore size distribution (IUPAC Technical Report). Pure Appl Chem. 2015;87(9-10):1051-1069.
[36]. Sing KSW, Everett DH, Haul RAW, Moscou L, Pierotti RA, Rouquérol J, et al. Reporting physisorption data for gas/solid systems with special reference to the determination of surface area and porosity (Recommendations 1984). Pure Appl Chem. 1985;57(4):603-619.
[37]. Bakti AI, Gareso PL, Rauf N. Characterization of active carbon from coconut shell using X-ray diffraction (X-RD) and SEM-EDX techniques. J Penelit Fis Apl. 2018;8(2)
[38]. Gibson JAA, Mangano E, Shiko E, Greenaway AG, Gromov AV, Lozinska MM, et al. Adsorption materials and processes for carbon capture from gas-fired power plants: AMPGas. Ind Eng Chem Res. 2016;55(13):3840-3851.
[39]. Saleem J, Zubair M, Shahid UB, Shakir S, Hussain M. High-performance activated carbon from coconut shells for dye removal: Study of isotherm and thermodynamics. Heliyon. 2024;10(17):e36399.
[40]. Haider R, Shahid MZ, Lock SSM, Hussein N, Ramli RM. Sustainable activated carbon derived from coconut shell and betel nuts for energy storage and environmental remediation. Diam Relat Mater. 2025;151:111669.
[41]. Heliani KR, Nurkholis A, Sugiarto Y, Suciyati SW. Screen printed carbon electrode from coconut shell char for lead ions detection. Int J Renew Energy Dev. 2024;13(4):576-583.
[42]. Azmi NZM, Ismail NA, Ahmad F. Enhancing the CO2 adsorption with dual functionalized coconut shell-hydrochar using Chlorella microalgae and metal oxide: Synthesis, physicochemical properties & mechanism evaluations. J Clean Prod. 2024;451:142184.
[43]. Yami TL. Low-cost chemically activated cow bone for fluoride removal from drinking water [dissertation]. Norman: University of Oklahoma; 2017.
[44]. Cazetta AL, Vargas AMM, Nogami EM, Kunita MH, Guilherme MR, Martins AC, et al. Thermally activated carbon from bovine bone: Optimization of synthesis conditions by response surface methodology. J Anal Appl Pyrolysis. 2014;105:177-185.
[45]. Shiryaev AA, Averin AA, Petrov DV. Microporosity and nanostructure of activated carbons: characterization by X-ray diffraction and scattering, Raman spectroscopy. Carbon. 2023;212:118143.
[46]. Muretta JE, Jones CW, Lively RP. Unique chemistry and structure of pyrolyzed bovine bone for enhanced aqueous metals adsorption. Waste Biomass Valorization. 2023;14(5).
[47]. Hart A, Omorogie MO, Wood J. Enhanced CO_2 adsorption using cow bone-derived activated char. J Clean Prod. 2023;414:137709.
[48]. Mpofu B, Mukaya HE, Nkazi DB. Mineral carbonation process of carbon dioxide using animal bone. Sci Prog. 2021;104(2).